Fracture simulations using large-scale molecular dynamics

Brad Lee Holian
Theoretical Division, Los Alamos National Laboratory, Los Alamos, New Mexico 87545

Ramon Ravelo
Department of Physics, University of Texas, El Paso, Texas 79968
(Received 9 June 1994; revised manuscript received 8 December 1994)

We report on recent molecular-dynamics (MD) fracture simulations of mode-I tensile loading at high strain rates. Because cracks emit sound waves, previous simulations became unreliable beyond one sound traversal time. Using massively parallel MD, we show how to eliminate unwanted boundary effects and study unimpeded crack propagation mechanisms. In order to represent tensile stress conditions near the crack tip, we employ uniaxial, homogeneously expanding periodic boundary conditions, examining the effects of strain rate, temperature, and interaction potential. Because our samples are sufficiently large, we see dislocations being emitted from the crack tip at nearly the shear-wave sound speed c_s. As they move many lattice spacings away from the crack, they slow down, finally moving at about $\frac{2}{3}c_s$. Each time dislocations are emitted, the crack tip "fishtails," and at sufficiently high strain, the crack can fork; dislocations can climb and become nucleation sites for additional microcracks. We find that we can suppress ductile behavior by including viscous damping in the equations of motion, thereby demonstrating a transition to brittle crack propagation as static, zero-strain-rate conditions are approached. Finally, we show that, by altering only the attractive tail of the pair potential, we can change a ductile material into a brittle one. Under dynamic crack propagation, the distinction between ductile and brittle behavior is blurred: in brittle materials, dislocations are asymptotically bound to the crack tip, while in ductile materials, they can escape.

I. INTRODUCTION

The first significant molecular-dynamics (MD) simulations of crack propagation were described in a landmark paper in 1976 by Ashurst and Hoover[1] and followed up by Moran.[2] They simulated plane-strain tensile loading in a two dimensional (2D) triangular lattice, containing either a notch or an elliptical hole. Since a total of about 1000 atoms were involved, the time and distance scales were extremely small, of the order of picoseconds and nanometers, invoking the oft-heard criticism of any attempt to relate MD simulations to "real-world" laboratory experiments. The interaction potential they used was intentionally simplistic—two quadratic regions of equal and opposite force constants joined at an inflection point (similar in shape to the familiar Lennard-Jones pair potential). Beyond these quadratic regions the potential is zero, representing a broken bond. As a consequence of this short-ranged, pseudoharmonic potential, very little blunting of the crack tip by emission of dislocations was seen, if at all—only for samples at initial temperatures that were a sensibly large fraction of the melting point. Moran correctly noted that, in addition, the narrowness of the sample transverse to the propagation direction might have inhibited realistic fracture mechanisms, and concluded that some more intelligent kind of boundary region, such as coupling to the continuum, was required in order to make further progress in MD simulations, at least for that generation of computers.

At about the same time, Mullins and Dokainish[3] proposed embedding an atomistic crack-tip region into a finite-element boundary region (much in the same spirit as Sinclair *et al.*, who proposed a much more complicated three-ring circus called "Flex-II,"[4] composed of a center ring—the atomistic crack-tip region—interacting with a ring of atoms farther out, which would themselves response to the outermost ring of elastic continuum atoms via a Green's function technique). Though this was a good idea and a valiant effort at the time, the samples were tiny 3D crystals composed of at most 400 atoms—a size which is totally inadequate to assure true independence from boundary effects. Also at that time, deCelis, Argon, and Yip proposed a constant-stress boundary condition,[5] which would eliminate some of the difficulties of the preceding methods, mainly in the transmission of dislocations emitted from the crack tip. Both these groups and the Paskin-Dienes group,[6] who were studying larger (10 000-atom) 2D systems, were able to observe either brittle or ductile behavior, depending on the potential used; for example, they noted that the Johnson alpha-iron potential[7] behaves in a brittle fashion, like the Hoover-Ashurst-Moran (HAM) potential. (These simulations and boundary treatments are discussed in some detail by Yip and Wolf in their review article on grain-boundary fracture.[8]) The constant-force boundary treatment has recently been used by Cheung and Yip in their study of the brittle to ductile transition in α-Fe.[9] Again, their calculations showed that dislocations are emitted from the crack tip, though the size of their 3D system (3000 atoms, or 10 nm on a side) is still far too small to achieve completely realistic crack propagation, including the nature of dislocation motion follow-

0163-1829/95/51(17)/11275(14)/$06.00

ing emission from the crack tip.

With the advent of massively parallel computers, simulations of millions of atoms are now feasible, as demonstrated by recent spallation simulations.[10] Our motivation here is to avoid, at least at first, the complex boundary treatments that have been employed in the past, opting instead for brute-force, massively parallel computations, where the systems are sufficiently large that disturbances emanating from the crack do not have time to reflect or transmit through boundaries and interfere with the propagation mechanisms. As we will see, of course, there are still limitations on the length of time over which even these large-scale simulations can be believed. In particular, the complexities introduced in 3D are beyond the scope of this paper.

In order to model the interior of an "infinite" (i.e., macroscopic) sample being pulled on at its edges, as in a tensile experimental setup, one can either attempt in an MD simulation to apply a constant force ("dead weight") to atoms in boundary reservoir regions, or one can constrain reservoir atoms to move at a constant velocity. In either case (as we have found by trying it out on these large systems), the "clamp" regions at the edges notify the interior notched region of this tension by sending out sound waves toward the notch at the center. After a time (of the order of twice the distance from the boundary to the notch, divided by the sound speed), the velocity profile across the sample can be well approximated by a linear function of distance from the notch outward, which corresponds to a constant initial strain rate. Following this acceleration phase, the material begins to be strained—that is, atoms are forced to expand homogeneously in tension. At a critical strain $\epsilon_{\rm crit}=\dot{\epsilon}t_{\rm crit}$ the crack begins to open up at the weakest spot, namely the tip of the notch, where the stress is concentrated. The critical time $t_{\rm crit}$ depends on the inverse of the imposed strain rate $\dot{\epsilon}$, so that lower strain rates, which are closer to those experimentally achievable in laboratory experiments, cause greater expense in MD simulations if nothing is done to circumvent this so-called "induction time."

The organization of the paper is as follows: in the next section we discuss the interaction potentials we have employed in our simulations, the crack and crystal configuration, and the simulation of constant strain rate by using expanding boundary conditions.[11] In Sec. III, we present our main results.[12] We will show that the opening of the crack causes emission of sound waves (which can rattle around in the computational MD volume if left unattended, even in systems where periodic boundary conditions are imposed). Later, plastic flow causes the crack tip to blunt, as dislocations are emitted from the crack tip and slippage occurs. The mobile dislocations, along with their attendant interactions with the sound waves, eventually reach the edge of the computational cell, where, if they are not absorbed somehow, they come back to the region of crack propagation and perturb it in an unphysical way. These considerations lead us to investigate system size effects and to attempt to make MD fracture simulations resemble more closely the interior response of a material to uniaxial tension by employing constant strain-rate initial conditions (a linear expansion-velocity profile) and absorbing reservoir-region boundary conditions to soak up sound waves and mobile dislocations.

We will next discuss the main differences in crack propagation found from constant strain-rate simulations using three different types of interatomic potentials. Following the discussion of these experiments, we show that we can turn an otherwise inherently ductile material into a brittle one by altering the attractive tail of the pair potential (from the minimum of the potential out to the cutoff distance). We also observe an unexpected mode of brittleness, in that the crack in this more brittle material is still able to generate dislocations, but they are almost immediately consumed by the crack, which zigzags to keep up with them. In other words, in a brittle material, we find that a more appropriate description for dynamic cracks is that dislocations are *asymptotically bound* to the crack tip, while in a ductile material, dislocations are *asymptotically free.*

Lastly, we show, by means of introducing viscous dissipation into a plane-strain fracture process, that ductility in crack propagation can be suppressed, even for a material that is otherwise inherently ductile. The artificial dissipation proves to be a useful tool for showing that the process of generating mobile dislocations at the crack tip is a thermally activated one, and that dynamic cracks can be qualitatively different from static ones. We present our conclusions and remarks for future work in Sec. IV.

II. SIMULATION METHODS

A. Interatomic potentials

In our simulations we have investigated the effect of interatomic potential on the dynamics of crack propagation by using two pair potentials—Lennard-Jones (LJ) 6-12 and Morse—and an analytic many-body embedded atom method (EAM) potential. As we will see later, the potential affects dislocation production (ductility) and crack propagation velocity. Elastic constants and other properties of the triangular 2D lattice are given for these potentials in Table I.

Throughout the paper, we use as units the atomic mass m, distance r_0 between neighbors in the zero-temperature and zero-pressure crystal, and bond energy ε; hence the unit of time t_0 is given by $\varepsilon=mr_0^2/t_0^2$. (The symbol ε for energy should not be confused with ϵ for strain.) The nearest-neighbor approximation has been used to compute all equation of state information.

The cohesive energy is given by

$$E_{\rm coh}=\tfrac{1}{2}N_1\varepsilon=\tfrac{1}{2}d(d+1)\varepsilon\ , \tag{2.1}$$

TABLE I. Elastic constants for LJ, Morse ($\alpha=4.5$), and EAM 2D crystals. Moduli: $B=$ bulk, $G=$ shear, $C_{11}=$ longitudinal ($V/N=$ volume per particle); sound speeds c are in units of $(\varepsilon/{\rm m})^{1/2}$.

	$BV/N\epsilon$	$GV/N\epsilon$	$C_{11}V/N\epsilon$	$c_{\rm bulk}$	$c_{\rm shear}$	$c_{\rm long}$
LJ	54	27	81	7.3	5.2	9.0
Morse	30	15	46	5.5	3.9	6.8
EAM	22	9	31	4.7	3.0	5.6

where $N_1=d(d+1)$ is the number of nearest neighbors in a close-packed crystal in d dimensions; for a pair potential, ε is the well depth. The volume per atom is given by

$$\Omega=\frac{V}{N}=g_d r_1^d \ , \tag{2.2}$$

where the nearest-neighbor spacing at zero temperature and pressure is $r_1=r_0$; for a pair potential, r_0 is the distance to the minimum of the potential; g_d is a geometric factor, $g_d=\frac{1}{2}(5-d)^{1/2}$. The ratio of the bulk modulus to the cohesive energy, a measure of the stiffness of the material in compression, is given by

$$2\alpha^2=\frac{m\omega_0^2 r_0^2}{\varepsilon}=\frac{mc_0^2}{\varepsilon}=d^2\frac{B_0\Omega_0}{E_{\rm coh}} \ , \tag{2.3}$$

where α is the stiffness parameter, m is the atomic mass, ω_0 is the fundamental harmonic frequency, $c_0=r_0\omega_0$ is the 1D (longitudinal) sound speed, and B_0 is the bulk modulus. These three parameters (r_0, ε, and α) determine the harmonic equation of state for continuous-potential materials; the first anharmonic correction is given by the cubic anharmonicity coefficient, which, for a pair-potential material, is defined as

$$\alpha_3\equiv-\frac{r_0}{2}\frac{\varphi'''(r_0)}{\varphi''(r_0)}, \quad m\omega_0^2=\varphi''(r_0) \ . \tag{2.4}$$

In 3D, the cubic anharmonicity is related to the pressure derivative of the bulk modulus dB_0/dP from static compression data, the slope s of the shock velocity vs particle velocity Hugoniot, and the thermal pressure dependence of the solid (via the Grüneisen parameter γ_0):

$$\alpha_3\approx\frac{3}{2}\left[\frac{dB_0}{dP}-1\right]\approx 6s-3\approx 3\gamma_0+1 \ . \tag{2.5}$$

In the following, energies are in units of ε and distances in units of r_0.

The Lennard-Jones pair potential ($\alpha\equiv 6$, $\alpha_3=10.5$):

$$\varphi(r)=r^{-12}-2r^{-6} \ . \tag{2.6}$$

In most of our simulations, we used a cubic spline, beginning at the inflection point, to make an intermediate-range version of the LJ potential (at normal density in 2D, this is a nearest-neighbor potential, while in 3D close-packed lattices, two shells of neighbors are included); details of the spline function are provided in Appendix A.

The Morse potential ($\alpha_3=\frac{3}{2}\alpha$; when $\alpha=6$, the Morse and LJ 6–12 potentials are virtually indistinguishable in the region near the minimum):

$$\varphi(r)=e^{-2\alpha(r-1)}-2e^{-\alpha(r-1)} \ . \tag{2.7}$$

Again, as in the LJ case, we used an intermediate-range version of this Morse potential.

Model analytic EAM:[13] The total potential energy of a system of N atoms, including contributions from a pair potential φ (we have used the intermediate-range LJ spline potential) and many-body embedding function $\mathcal{F}$ (the fractional pairwise contribution $0<\chi\le 1$ approximates the ratio of vacancy formation energy to cohesive energy), is given by

$$\begin{aligned}
\Phi&=\sum_{i=1}^{N}\left[\frac{1}{2}\chi\sum_{j\neq i}\varphi(r_{ij})+(1-\chi)\mathcal{F}(\bar\rho_i)\right] \ , \\
\mathcal{F}(\bar\rho_i)&=\frac{E_{\rm coh}}{\bar\rho_0}\bar\rho_i\ln\bar\rho_i \ , \\
\bar\rho_i&=\sum_{j\neq i}w(r_{ij}) \ , \\
w(r)&=\begin{cases}\dfrac{\bar\rho_0}{d(d+1)}\left[\dfrac{r_m^2-r^2}{r_m^2-1}\right]^2, & 0<r<r_m \\ 0, & r\ge r_m \ .\end{cases}
\end{aligned} \tag{2.8}$$

The force on atom i is

$$\begin{aligned}
\mathbf{F}_i&=-\frac{\partial\Phi}{\partial\mathbf{x}_i} \\
&=-\sum_{j\neq i}\{\chi\varphi'(r_{ij})+(1-\chi)[\mathcal{F}'(\bar\rho_i)w'(r_{ij}) \\
&\qquad +\mathcal{F}'(\bar\rho_j)w'(r_{ji})]\}\frac{\mathbf{x}_{ij}}{r_{ij}} \ ,
\end{aligned} \tag{2.9}$$

$$\mathcal{F}'(\bar\rho_i)=\frac{d\mathcal{F}}{d\bar\rho_i}=\frac{E_{\rm coh}}{\bar\rho_0}(\ln\bar\rho_i+1), \quad \mathcal{F}'(\bar\rho_0)=0\Longrightarrow\bar\rho_0=\frac{1}{e} \ .$$

From this, we see that in the approximation of only nearest-neighbor interactions, the pressure at normal density and zero temperature is zero, and the negative of the total potential energy per particle is the cohesive energy. Thus, this model analytical EAM is easily characterized for any metal. An alternative form for the embedding function $\mathcal{F}$, which is perhaps more realistic at moderate compressions, but which we did *not* use in these fracture studies, is given by

$$\mathcal{F}(\bar\rho_i)=\frac{E_{\rm coh}}{\bar\rho_0}(\bar\rho_i-\sqrt{\bar\rho_i}), \quad \bar\rho_0=\tfrac{1}{4} \ . \tag{2.10}$$

In addition to these potentials, we also employed a shorter-range LJ potential, where the spline was begun at the minimum of the potential, in order to see how modifying the attractive part of the potential would affect dislocation emission. As will be discussed later, the anharmonicity of the attractive part of the potential plays a crucial role in dislocation production. Details of these modifications as well as analytic forms of other potentials (HAM[1,2] and Johnson[7]) discussed in the text are to be found in Appendix A.

B. Setup of the simulations (initial and boundary conditions)

The systems studied consisted of rectangular samples of the 2D triangular lattice, with aspect ratios (horizontal:vertical length) between 1 and 2 and system sizes of 16 000–300 000 atoms. A triangular notch with a ratio of width:depth of 1:5 was cut in the middle of the lower horizontal boundary; notch depths varied between

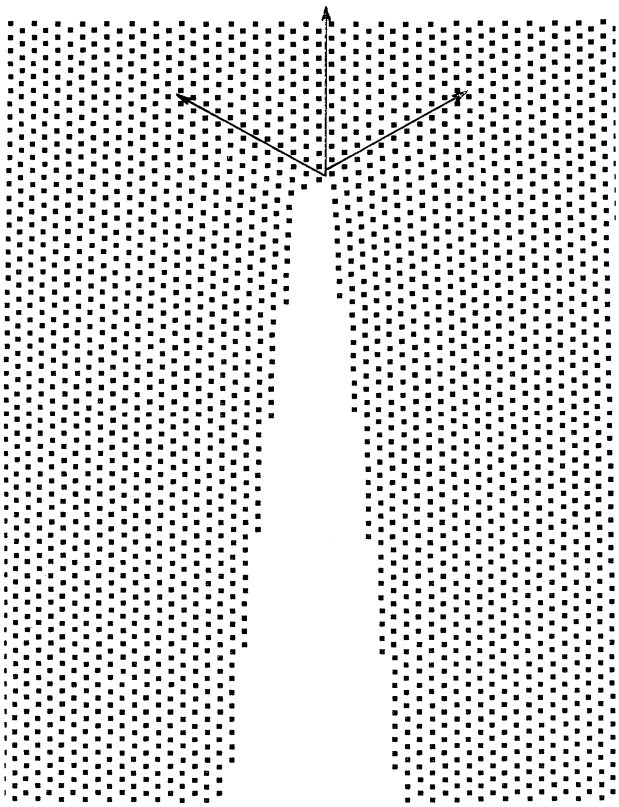

FIG. 1. Atomic region around a triangular notched crack, showing its orientation with respect to the triangular lattice and dislocation slip planes in this geometry.

10 and 50 atomic spacings. In a few cases, an elliptical hole, oriented transverse to the strain, was cut out of a 1:2 aspect ratio bulk sample; major axes ranged from 6 to 68, with minor axes of 1–1.5. In all simulations reported here, the notch or hole points in the direction of a close-packed (slip) line in the triangular lattice, which is the natural direction for cleavage. Figure 1 shows the geometry and orientation of a typical notch as well as the slip lines along which dislocations propagate.

We employed uniaxial, homogeneously expanding periodic boundary conditions, which mimic the behavior in the interior of a large sample that is expanding at constant energy. This kind of boundary condition was first proposed to study fragmentation of a fluid.[11] A constant Lagrangian strain rate (in the x direction, say) is imposed by adding to the x component of each atom's thermal velocity a term proportional to its x coordinate, namely $\dot{\epsilon}x$. The sidelength of the computational box in the x direction increases with time as

$$L_x(t)=L_x(0)[1+\dot{\epsilon}(0)t] , \tag{2.11}$$

so that, for example, the right-hand periodic boundary, initially located at $\frac{1}{2}L_x(0)$, moves at a constant velocity $\frac{1}{2}\dot{\epsilon}(0)L_x(0)$. When particles cross the periodic boundaries, their velocities must be adjusted in magnitude by twice the boundary velocity, with the sign chosen so as to preserve the sense of expansion. Wagner, Holian, and Voter subsequently verified by MD simulations that spallation experiments, which cause fracture by shock waves and their subsequent release, produce just such linear velocity profiles about the spall plane.[10] They then used this same kind of homogeneous expansion to map out the failure stress (and strain) as a function of strain rate.

Of course, in a simulation of fracture under typical laboratory conditions, this constant expansion cannot go on forever; instead, it represents the transient response to a suddenly imposed tensile force at the edge of a macroscopic sample. For example, we do not expect that constant strain-rate simulations are capable of extracting a steady crack propagation velocity that results from a dead weight applied at the boundary, or the equivalent (for small strains) of a constant displacement. If a constant strain-rate experiment is pursued, the sample is strained beyond its elastic response, so that the crack begins to open up. One by one, a series of instabilities will be probed, until eventually, the material reaches the ultimate instability—bulk mechanical failure.

The long-time behavior of a crack under steady loading at infinity can be studied by constant displacement simulations (zero strain rate). The sample with either an elliptical hole or a notch at a free surface can be strained suddenly to a supercritical value. This induces a rarefaction wave at surfaces that are approximately orthogonal to the applied strain. An alternative procedure, which avoids this additional perturbation to the system, is to ramp up the strain gradually at a small rate, allowing the free surfaces to relax to zero stress. Then, when a critical strain is achieved, the crack begins to move: a plot of atomic velocities transverse to the direction of crack propagation shows distinctly the breaking of the first bond, which generates a sound wave. A short time thereafter, the strain can be frozen at a small value above critical by subtracting off the linear velocity profile associated with the slow expansion:

$$u_i'=u_i-\dot{\epsilon}(t)x_i, \quad \dot{\epsilon}(t)=\frac{\dot{\epsilon}(0)}{1+\dot{\epsilon}(0)t} . \tag{2.12}$$

However, we emphasize that with any supercritical strain, even if arrived at by this gentle ramping-up procedure, the crack is dynamic, and its characterization as brittle or ductile may be different from a static consideration.

We used strain rates of 10^{-3} and $10^{-4}t_0^{-1}$ in most of our fracture simulations. The equations of motions were integrated using the Størmer (Verlet) central-difference method[14] with a time step of $0.02t_0$, or about $\frac{1}{20}$ of the Einstein vibrational period. Consistency in the time evolution of the cracks was checked by using half and one-quarter of this value. Unless otherwise noted, the initial temperature T_0 of the samples was virtually zero ($10^{-6}T_{\text{melt}}$). Our simulations were carried out on the Connection Machine CM-200 for smaller systems (up to 65 000 atoms) and for larger systems (up to 300 000 atoms) on the CM-5.

In the next section we discuss the effect of strain rate, interatomic potential, notch size and shape, and viscous

damping on the dynamics of crack propagation and dislocation production.

III. RESULTS

Simulations with the LJ potential and a strain rate of $\dot{\epsilon}=10^{-2}t_0^{-1}$ (about 10^{10} per second in engineering units), although well below the sonic expansion limit, lead to catastrophic failure of the sample with no crack propagation. At an initial temperature of about one-fourth melting, ductile holes were nucleated throughout the sample after a time of about $3t_0$ (a strain of about 3%), wherever the local thermal fluctuations led to low density. Rather than opening up the crack at the notch tip, the entire sample pulled apart plastically, like taffy. Reducing the temperature to almost zero led to results that were qualitatively similar to the higher-temperature simulations.

At a strain rate one order of magnitude lower (10^{-3}) and at nearly zero temperature, we found that the crack began to open up in a brittle fashion, namely, by bond breaking at the notch tip in response to a critical stress concentration. The induction time to reach this critical strain of 2% was about $20t_0$. At an even lower strain rate of 10^{-4}, the same critical strain is reached at a time of over $200t_0$. Sound waves were emitted by the bond-breaking process (the measured velocity of the waves was about 90% of the longitudinal sound speed). Soon after the crack opened up by about 10 lattice spacings in the forward direction, pairs of dislocations were emitted from the crack tip, moving off along the slip lines at $\pm 60°$ at about 90% of the shear-wave sound speed (c_s). These mobile dislocations themselves appear to emit sound waves as they go, leaving behind wakes like speedboats in water, and slowing down to about two-thirds of c_s far from the crack.

Accompanying the dislocation emission every 10 or so atomic spacings, the crack zigzags slightly, and finally, at a strain of a little over 3% for LJ crystals, it bifurcates (no such forking occurs for the softer Morse and EAM systems). This forking instability sets in at a particular supercritical strain that seems to be strain-rate independent. A series of closely spaced snapshots reveals that branching sometimes occurs in an asymmetric way: instead of opening up on both sides, a slow dislocation is emitted on one side, which then climbs up as many as ten slip planes and then forms a nucleation site for the second branch.

As the simulation of crack propagation proceeds, sound waves that have been emitted from the opening of the crack tip return to the central crack region—either by reflection from free boundaries or transmission through periodic boundaries. One can ask whether these sound waves perturb the propagation of the crack in an unphysical way; to assess this, we carried out simulations for systems differing in transverse width.

A. System size effects

We studied the dependence of these fracture simulations on system size (or equivalently, on boundary conditions) by comparing the results of imposing a strain rate of $\sim 10^{-4}$ on two LJ crystals differing only in their widths transverse to the notch direction. The first was composed of 300 000 atoms and had an aspect ratio of unity, while the second was twice as wide and contained 600 000 atoms. The two systems are shown at a time of $312t_0$ (approximately $75t_0$ after crack initiation) in Fig. 2. In Fig. 2(a) (300 000 atoms), the full periodic system is shown. Particles are colored by a rainbow ranging from deep blue for the maximum leftward velocity of $-u_p$, to green for zero velocity, to bright red for a velocity of $+u_p$, where $\dot{\epsilon}=2u_p/L_x$ is the expansion velocity of the periodic boundaries consistent with the initial strain rate and L_x is the periodic length in the transverse (x) direction. In Fig. 2(b) (600 000 atoms), only the central half is shown at the same scale (the periodic boundaries themselves are outside the field of view; the velocities are colored as in Fig. 2(a)).

In Fig. 2(b), the dislocation cores from the forked crack show up as dark clusters moving out at $\pm 60°$ from the vertical (crack-propagation direction). The dark, flat patterns immediately above the forked crack are sound waves or acoustic interference caused by slippage accompanying the dislocation cores. The sound waves emitted from the crack opening due to bond breakage have already bounced off the top free surface and appear as a family of concave upward arcs that intersect concave downward arcs from later bond-breaking events. In contrast to the larger system, the lower half of the map for the smaller system in Fig. 2(a) is mottled, indicative of sound wave interference from the periodic image cracks on either side. This interference has prevented the crack in the smaller system from forking; fewer dislocations have been emitted, and the crack is narrower, though the crack lengths are similar.

The observed differences in crack morphology for the two system widths are much too large to be accounted for by initial conditions, since in both cases, the initial temperature is virtually zero ($10^{-6}T_{\text{melt}}$). Moreover, up until this time, a series of snapshots of the two systems taken every $25t_0$ look completely identical. Figures 2(a) and 2(b) clearly show that if sound waves generated by the crack are not absorbed at the boundaries, there is a limiting time for unperturbed crack propagation. This limiting time is the sound traversal time, $t_L=L_x/c$, where c is the sound speed. If longer simulation times are required, care must be exercised in treating the boundary regions; otherwise, conclusions drawn from samples that are too narrow will be qualitatively, as well as quantitatively, wrong. To this end, in Appendix B we describe special atomistic reservoirs, the purpose of which is to reduce the influence of reflected or transmitted disturbances on the crack-tip region.

In Fig. 2(c), we show the results of a successful fracture simulation in a 250 000-atom LJ system, using these absorbing boundaries (20 atomic layers wide, with a gradient in viscous damping coefficient of about $1/r_0t_0$), where the time after crack initiation ($75t_0$) is significantly longer than t_L ($\sim 60t_0$). The strain in this simulation was built up at a gradual rate of 10^{-3} and then frozen at 3%; note therefore that the velocity in the applied strain direction is mostly green, indicating zero expansion ve-

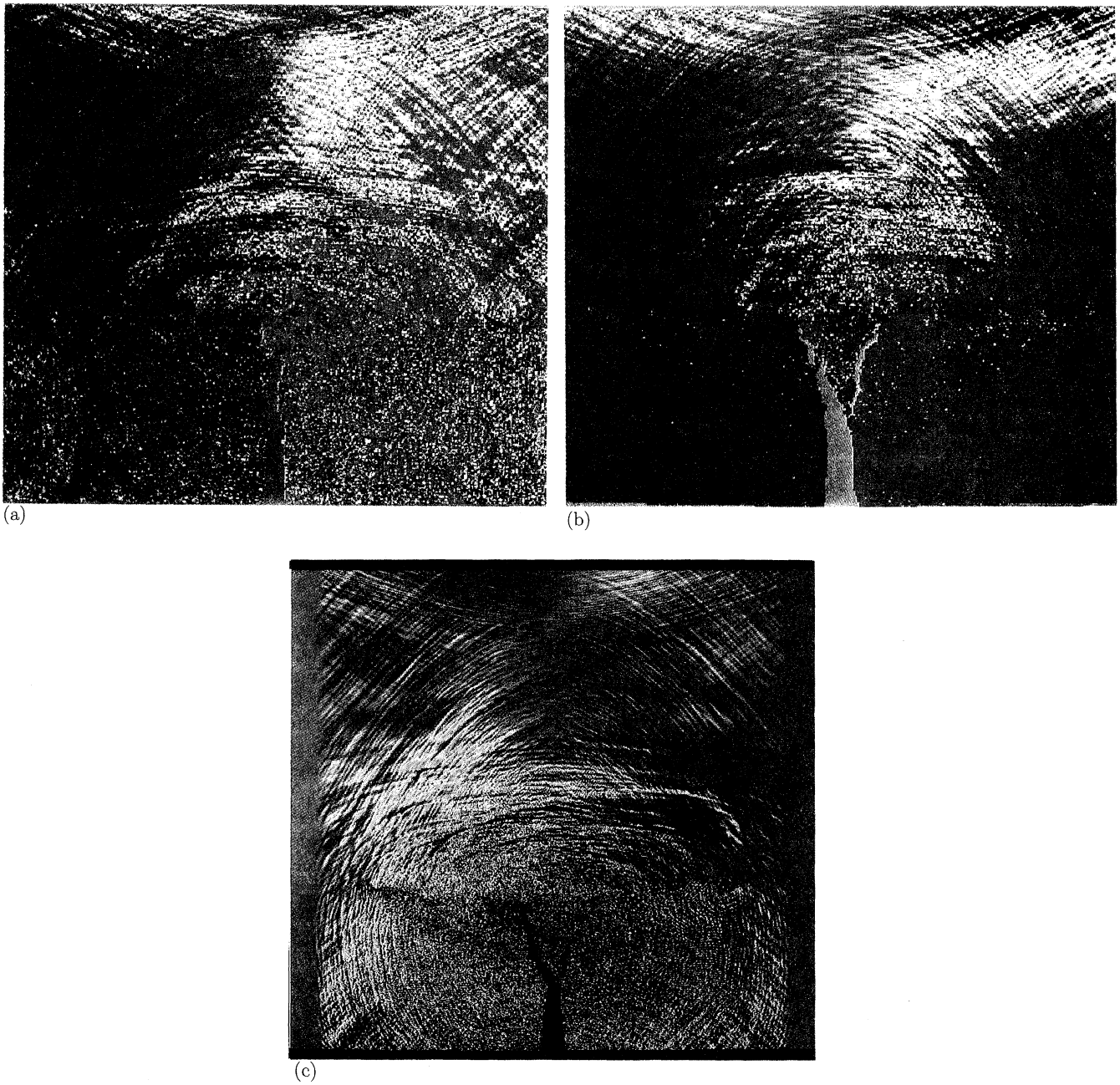

FIG. 2. Comparison of system-size (periodic boundary condition effects) on crack propagation at constant strain rate (10^{-4}) in the 2D LJ crystal at time $t=312t_0$ for two system sizes: (a) 300 000 atoms, aspect ratio (horizontal/vertical) = 1, entire sample shown; (b) 600 000 atoms, aspect ratio =2, middle half of sample shown—same area as in (a). Constant strain simulation (3%) for 250 000 atoms at $t=75t_0$ after crack initiation is shown in (c); ramped viscous damping is applied at left and right boundary regions (each 20 atomic layers thick).

locity [in contrast to the constant strain-*rate* simulations shown in Figs. 2(a) and 2(b)]. The crack has forked in an unhindered fashion, as in Fig. 2(b). A movie of the crack propagation, of which Fig. 2(c) is the final frame, demonstrates that all sound waves have been absorbed at the boundaries, and that no disturbances have returned to the central crack region.

The quantitative results in this paper, wherever these absorbing boundaries were *not* used, were obtained from early-time crack-propagation measurements (i.e., times less than t_L beyond crack initiation).

B. Crack propagation measurements: LJ, Morse, and EAM systems

As mentioned in Sec. II A, in order to test the effect on the dynamic crack process of the intrinsic brittleness or

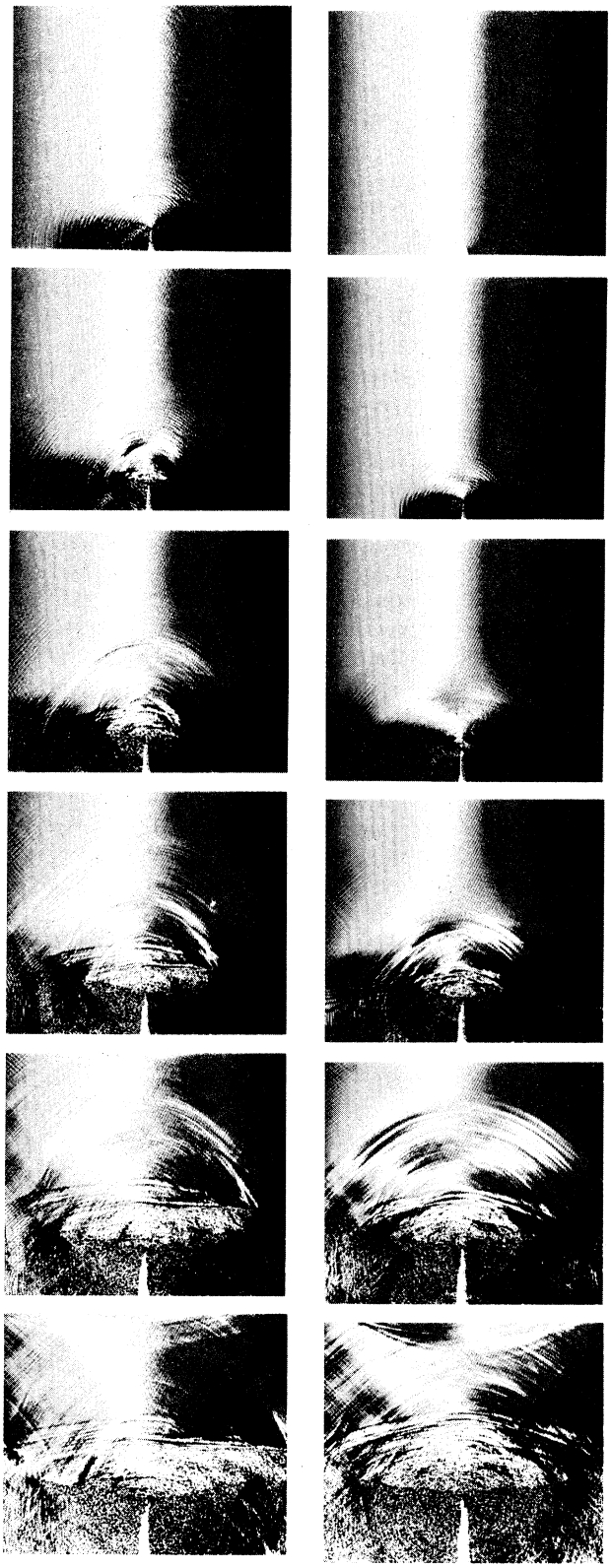

FIG. 3. MD simulations of 2D fracture at constant strain rate (10^{-4}) for Morse pair potential (time sequence $t=275-400t_0$ on left-hand side) and many-body EAM potential (on right-hand side, $t=245-356t_0$).

ductility of the interaction potential, we studied, in addition to the LJ pair potential, the Morse pair potential and the EAM many-body potential, which is appropriate to metals and has significantly lower vacancy and surface formation energies. The Morse potential was chosen to mimic the EAM equation of state, including bulk sound speed, which is roughly half that of the LJ system. (These potentials are described, along with their affect on plastic flow, elsewhere.[13])

In Fig. 3, we show a pair of time sequences of maps of the x component of particle velocity for the Morse and EAM crystals (300 000 atoms, aspect ratio of unity), at a homogeneous strain rate of $\dot{\epsilon}=10^{-4}t_0^{-1}$ for Morse and 1.12×10^{-4} for EAM. Note that the critical strain for initiation of the propagation of the crack is reached first in the EAM system, beginning at a time of about $t=220t_0$ for a critical strain of 2.5%; for Morse, the time is 290 and the strain is 2.9%. For the EAM potential, the energy required to form new free surfaces is lower than for Morse. At the end of the sequence, the Morse crack is about 15% longer. The EAM crack generates an extra pair of dislocations, which absorb energy from the propagation process. The EAM system, however, does not differ appreciably in its ductility from the LJ and Morse systems under these dynamic crack propagation conditions.

For the LJ, Morse, and EAM systems at strain rates from 10^{-2} to 10^{-4}, the critical strain for initiation of crack propagation is nearly independent of strain rate. At the lowest strain rate, the order of crack initiation among the three interaction potentials can be estimated by the Griffith criterion, a simple energy balance between the elastic strain energy, which is proportional to the longitudinal modulus C_{11} times the square of the critical strain ϵ_{crit}, and the energy required to form a surface per unit length, γ. In Table I, we present the 2D elastic constants and sound speeds for the three interaction potentials. The surface energies are roughly $\gamma_{\text{LJ}}\sim\gamma_{\text{Morse}}\sim2\gamma_{\text{EAM}}$, because the reduced density near a free surface of the many-body EAM has a pronounced effect on γ compared with the two pair potentials. Hence, for a constant notch shape (narrow triangle), we can rank the potentials according to $\epsilon_{\text{crit}}\sim(\gamma/C_{11})^{1/2}$, i.e., Morse:EAM:LJ=1.34:1.11:1. The observed results are reasonably close, as shown in Table II, where we summarize the strain-rate dependence of the critical strain for atomistically sharp cracks.

In Fig. 4, we present crack velocities (the slope of measured crack-tip positions), whose differences can be explained on the basis of sound speeds of the three materials. These materials are all ductile, at least at these strain

TABLE II. Critical strain (%) for initial crack motion as a function of potential and strain rate (in units of t_0^{-1}).

Strain rate →	0.0020	0.0010	0.0005	0.0001
LJ	2.6	2.0	2.45	2.2
Morse	3.4			2.9
EAM	3.2			2.5

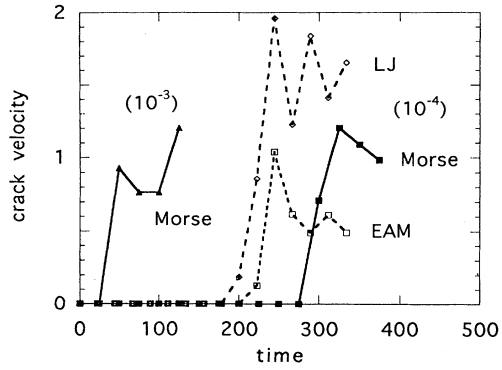

FIG. 4. Crack velocity versus time for 2D Morse, EAM and LJ crystals as computed from crack extension (strain rates in parentheses).

rates. Note that the crack velocity is a weakly decreasing function of strain rate, due to the higher rate of dislocation production. Also, the LJ crack velocity exhibits markedly oscillatory behavior. Velocity measurements of various types are summarized in Table III for the three interaction potentials at the lowest strain rate. The peak crack velocity appears to be consistently about one-third the shear-wave sound velocity (c_s) for all three potentials, while the average (plateau) value is lower, especially for the EAM crystal. The sound pulse that emanates from the early bond-breaking (brittle) phase of crack initiation moves out at 90% of the longitudinal speed for all three potentials. This is consistent with the rather long wavelength that is seen, namely about five interatomic spacings, as well as the tensile strain of 2–3%. The velocities of the dislocations emitted from the crack tip, when they have moved well away from the crack and have separated from each other (by tens of lattice spacings), approach a constant speed of about two-thirds of c_s.

Dislocations emitted per unit crack length for EAM, Morse, and LJ crystals are 0.11, 0.07, and 0.05, respectively. On that basis, we could conclude this is also the order of intrinsic ductility in these three materials; on the other hand, the *rate* of dislocation emission is highest for the LJ crystal, followed by EAM and Morse. The emission rate decreases by a factor of 4 when the strain rate drops by a factor of 10. Nevertheless, the crack velocity does not increase very much as strain rate drops.

TABLE III. Sound-pulse, dislocation, and crack velocities in units of $(\varepsilon/m)^{1/2}$ for LJ, Morse ($\alpha=4.5$), and EAM 2D crystals at a strain rate of $10^{-4}t_0^{-1}$ (λ=measured peak-to-peak wavelength at front in units of r_0).

	v_{pulse} (λ)	$v_{\text{dislocation}}$	v_{crack} (average)	v_{crack} (peak)
LJ	8.1 (5.5)	3.3	1.6	2.0
Morse	5.9 (4.4)	2.7	1.1	1.2
EAM	5.2 (5.2)	2.0	0.6	1.0

C. Effect of the attractive region of the potential upon ductility

At the strain rates investigated, we found these three materials (LJ, Morse, EAM) to be ductile. Only by adding viscous dissipation to the atomic equations of motion (discussed later), were we able to get completely brittle fracture. However, other potentials, such as the pseudoharmonic (HAM[1,2]) and Johnson α-Fe,[7] appear to be intrinsically brittle. Why is this so? We wish to ascertain what aspect of these potentials is crucial to their inability to produce dislocations during the fracture process, at least for low supercritical strains. As we have shown in Sec. II A, a continuous pair potential can be characterized by at least three quantities: distance and energy scales (r_0, the minimum of the potential, which determines the normal density and ε, the well depth of the potential, which determines the cohesive energy) and $2\alpha^2$, the curvature at the minimum of the potential (ratio of bulk modulus to cohesive energy). The quantities r_0, ε, and $2\alpha^2$ determine the condensed-matter equation of state, at least for low temperatures and densities near normal. It is our view that modifications to the attractive tail beyond the potential minimum can give rise to nonequilibrium behavior in expansion, including intrinsic brittleness or ductility.

We can construct a variety of short- to intermediate-range potentials using, for example, cubic spline functions that begin at $r_s \geq r_0$ and terminate at the maximum interaction distance r_m with zero potential and force. At r_s, we require that the pair potential, force, and curvature be continuous, thereby leaving the compressed equation of state unchanged, at least in the nearest-neighbor approximation. At one end of the spectrum of potentials we can construct this way is the attractive part of the HAM potential beginning at $r_s=r_0$. We expect this short-range modification to exhibit brittle behavior at zero temperature, just like the full HAM potential. Moreover, this modification—in contrast to the full HAM potential—preserves, in the nearest-neighbor approximation, the correct anharmonic behavior in compression, including realistic values for the pressure derivative of the bulk modulus, the slope of the shock Hugoniot (shock velocity versus particle velocity), and the thermal part of the solid pressure (via the Grüneisen parameter), as well as the correct sign of the thermal expansion. At the other end of the spectrum of potentials, the intermediate-range LJ spline potential, where r_s is the inflection point, $(\frac{13}{7})^{1/2}r_0=1.109r_0$, exhibits ductile dynamic fracture behavior, as does the full LJ potential. In Fig. 5, we present the LJ potential and these modified LJ potentials.

With this discussion, we are now in a better position to see how the Johnson α-Fe potential, whose fracture behavior at zero temperature is brittle, fits into this picture. The Johnson potential is very harmonic, having a cubic anharmonicity of $\alpha_3=2.62$, and very short ranged, going smoothly to zero just beyond the closely spaced first and second neighbors in the 3D body-centered cubic lattice. In Fig. 6, we show that the compressive part of the Johnson potential can be well approximated by a

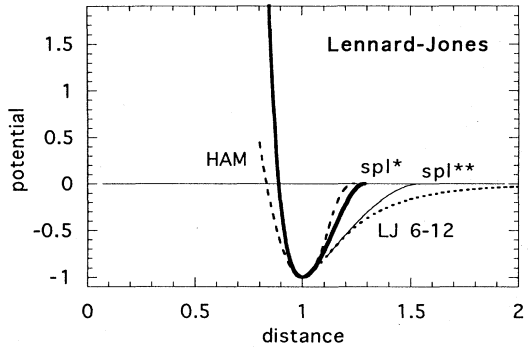

FIG. 5. Lennard-Jones potentials: "LJ 6–12" is the full potential (dotted line), "spl**" is the intermediate-range cubic spline (light solid line), "HAM" is the Hoover-Ashurst-Moran potential (dashed line), and "spl*" is the short-range cubic spline (heavy solid line).

Morse potential with $\alpha=5$ ($\alpha_3=7.5$); in expansion, it can be represented by the short-range cubic spline beginning at the minimum. The fact that the intermediate-range Morse spline potential ($\alpha=4.5$) is ductile leads us to speculate that brittleness or ductility is determined within a very narrow range in the attractive part of the potential, where the attractive force between atoms is strongest.

We tested this hypothesis using the short-range, cubic-spline version of the LJ potential. We placed a zero-temperature sample of 16 000 atoms under periodic boundary conditions, cut an elliptical hole in the center aligned perpendicular to the strain direction (radii 10 and $2r_0$), and imposed a sudden uniaxial strain of 3%. (The critical strain was observed to be about 2.8% under sudden strain, rather than 3.15% observed for gradual ramp-up of the strain.)

In Fig. 7, we show a sequence of snapshots detailing the brittle opening of the crack. We had expected to see a sharp, straight crack. To our surprise, the fracture was much more complex, in that dislocation pairs could be seen to be forming, but as soon as they did, the crack would jump over and absorb one of them, healing up the other. Thus, the crack was seen to oscillate back and forth—a common feature in brittle fracture—though in this case, the amplitude is only one atomic layer. At a higher strain of 6%, the dislocations could get a little farther away from the crack, but the crack would fork and chase after the pair of them. We see, therefore, that the difference between brittle and ductile behavior in dynamic cracks is a subtle one: in a brittle material, the dislocations are *asymptotically bound* to the crack while in a ductile material, they are *asymptotically free*. It is largely a matter of the difference between the formation energy of the crack surface and formation energy of the dislocation; in a ductile material, it is easy to make free-moving dislocations, while in a brittle material, even if dislocations are generated, the crack can follow the dislocation more easily.

We conclude that the larger the attractive force at the critical strain, the more likely it is that the material will be brittle. We observe that the size of the dislocation core—4–5 atomic spacings for the short-range LJ spline, compared to 7–8 for the intermediate-range LJ spline—and the inertia of the dislocation, i.e., its mobility, are inversely proportional to this maximum attractive force, while the surface energy is determined primarily by the well depth of the potential. In the brittle case, the dislocations are smaller (more discrete) and therefore more "massive" than in the ductile case. Work in progress focuses on making these arguments more quantitative.

Recently Zhou, Carlsson, and Thomson suggested that the unstable stacking fault energy determines intrinsic ductility (the so-called ZCT criterion[16]). Our emphasis on the maximum attractive force of the potential appears to converge with their view. However, direct comparison with their work is difficult, since the potentials they used were considerably softer than any that we used. Moreover, they considered static (zero-velocity, zero-temperature) cracks in a material infinitesimally above the critical strain—much in the same spirit as our artificial viscous damping experiments, to be described next. On the other hand, most of our calculations were at either a finite strain rate or a finite strain above critical. Since they assume a single dislocation is emitted, while we see often that pairs are emitted almost simultaneously, it is clear that dynamical effects—including finite "temperature" at the crack tip—are important for crack propagation at a finite velocity. In a future paper, we will report on comparisons of our MD results to their work.

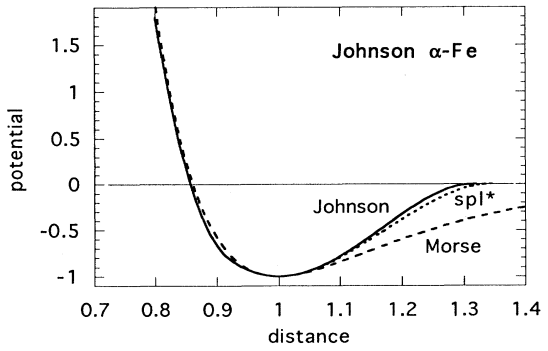

FIG. 6. Johnson α-iron potential (solid line); Morse potential ($\alpha=5$, dashed line); "spl*" is the short-range cubic spline.

D. Effect of viscous dissipation upon ductility

In the foregoing fracture simulations, we observed that the nonequilibrium (i.e., transient) kinetic temperatures of atoms in highly localized regions—near the crack tip and mobile dislocation cores—were surprisingly hot, approaching the equilibrium melting temperature (although the samples always remained completely crystalline, apart from the dislocations). We therefore undertook the study of uniaxial plane-strain crack propagation with varying rates γ of viscous dissipation in the equations of motion for all the atoms (the symbol γ for viscous dissipation should not be confused with that for surface energy). Our hypothesis was that if γ were made sufficiently

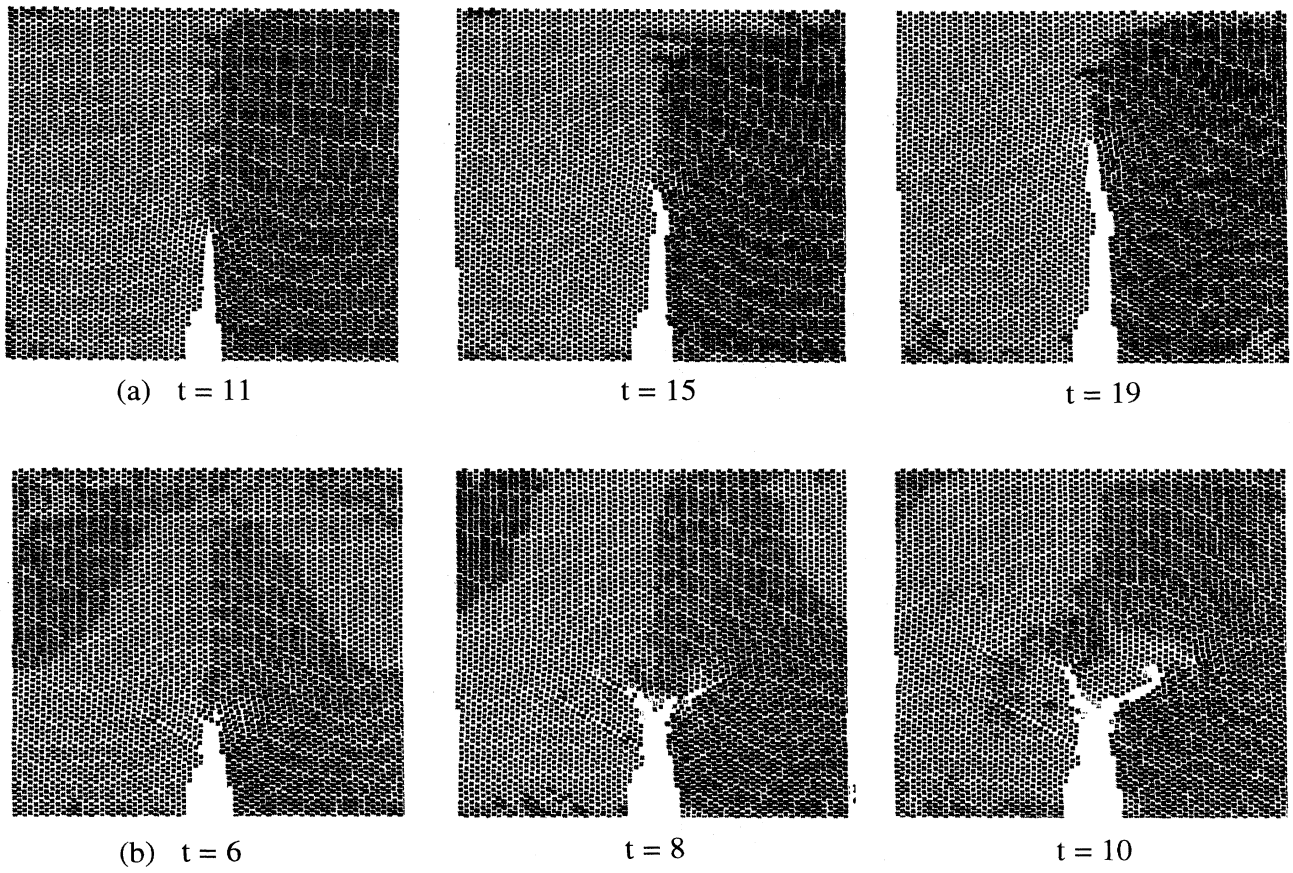

FIG. 7. Brittle fracture (*without* viscous dissipation) in a 2D crystal whose atoms interact via the short-range LJ spline potential. (a) Grain map emphasizing dislocation cores (atoms colored by 60°-periodic rainbow according to orientation of hexagon of nearest neighbors: red at vertical, green at 30° to right, blue at 60°) shown for initial strain of 3% in the horizontal direction at $t=11$, 15, $19t_0$; (b) initial strain of 6%, for $t=6$, 8, and $10t_0$.

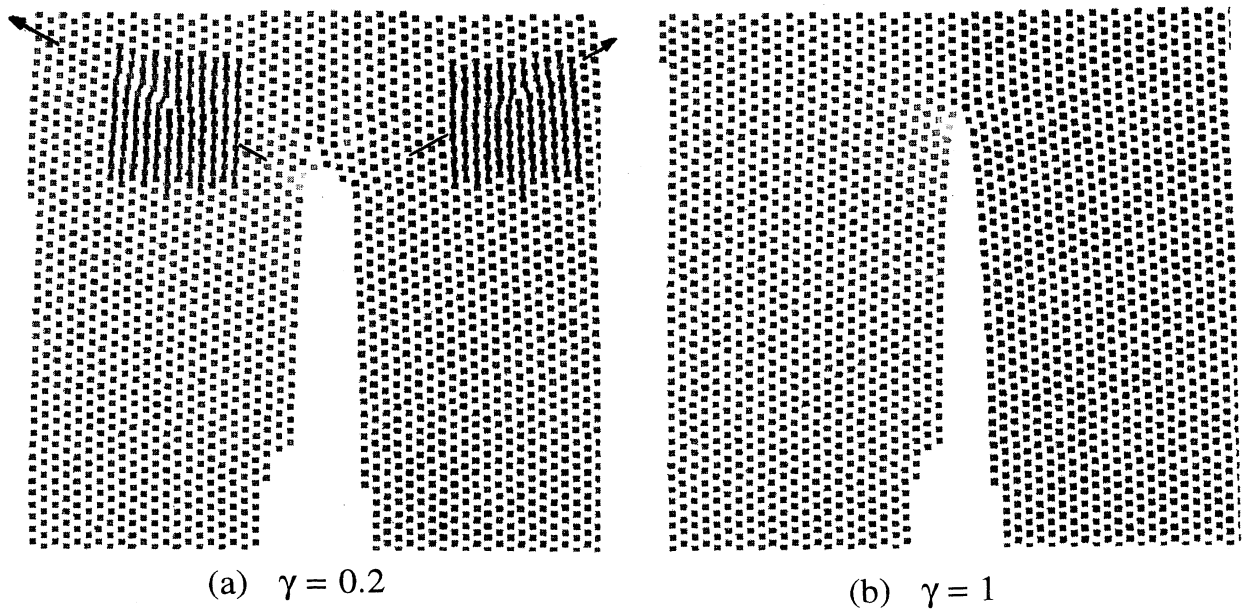

FIG. 8. Effect of viscous dissipation on ductility (grain map as in Fig. 7) in the 2D LJ crystal, prestrained in the horizontal direction to 5%; (a) viscous damping coefficient $\gamma=0.2$ at $t=22t_0$ (note pair of dislocations along $\pm 60°$ slip lines); (b) $\gamma=1$ at $t=30t_0$ (brittle crack).

large, the heating near the crack tip, where bonds have been broken and potential energy has been converted to kinetic, would be dissipated so quickly that dislocations could not be formed to blunt the tip. Since dislocations require energy to be generated, as well as to be made mobile, the viscous damping thus could be viewed as a competing dissipation mechanism, allowing brittle crack propagation. We emphasize that we used this dissipation merely as an artifice for investigating the thermal activation process, as distinguished from the continuum picture of Langer and Nakanishi,[17] where their damping is meant to account for a variety of underlying dissipative mechanisms.

We introduce homogeneous viscous damping into the equations of motion via the irreversible Berendsen thermostat:[18]

$$m\ddot{\mathbf{x}}=\mathbf{F}-\gamma\left[1-\frac{T_0}{T}\right]m\dot{\mathbf{x}}\ , \tag{3.1}$$

where γ is the viscous damping rate at zero temperature, T_0 is the temperature of the thermal bath, and T is the instantaneous kinetic temperature for N atoms in d dimensions:

$$dN\,kT=\sum_{i=1}^{N} m_i|\dot{\mathbf{x}}_i-\dot{\epsilon}x_i\hat{\mathbf{x}}|^2\ . \tag{3.2}$$

(In the case of constant strain, the local expansion velocity is zero, since $\dot{\epsilon}\equiv 0$.) At $T_0=0$, the usual viscous damping equations of motion are recovered. Berendsen *et al.* motivated these equations of motion by imagining that the atoms are massive solute particles immersed in a sea of light solvent particles. Such a picture has recently been used to model thermal motion of metal ions in an electron gas,[19] where local viscous (Berendsen) damping in the equations of motion can be justified by electron-phonon coupling between the electron gas and the ions. In LJ units of t_0^{-1}, this coupling constant corresponds to $\gamma\approx 0.1$ for (3D) copper, which is well below critical damping for harmonic LJ crystals: $\gamma_{\rm crit}=2\omega_0\sim 17$.

We chose to study first a small LJ system (16 000 atoms), prestrained to about twice the threshold value (5%), with an elliptical hole cut out in the middle, an initial temperature set to $T_0=0$, and $\gamma=0.1$. The resulting fracture was ductile, as was the case when γ was increased to 0.2. However, in the case of $\gamma=1$, the crack opened up in a completely brittle manner; no dislocations could be generated at the crack tip, which remained atomically sharp during bond breaking (see Fig. 8). With $\gamma=1$ and $kT_0/\epsilon=0.1$ (about one-fourth the LJ melting temperature in 2D), ductile behavior—dislocation generation—was seen once again, with new cracks opening up away from the original crack tip at dislocation cores that had escaped along the $\pm 60°$ slip lines. This leapfrogging appeared to occur in much in the same manner as forking we observed at lower temperatures under homogeneous strain-rate conditions.

By increasing the initial strain to 10% ($T_0=0$), so that more energy would be released upon bond breaking, a value of $\gamma=1$ was no longer sufficient to ensure brittle behavior; for this case, a value near $\gamma=3$ was required.

TABLE IV. Crack velocities in units of $(\epsilon/m)^{1/2}$ under artificial viscous damping (coefficient γ, in units of t_0^{-1}) in the LJ crystal, at constant strain of 5%.

γ	$v_{\rm crack}$ (average)	$v_{\rm crack}$ (peak)
0	1.6	2.0
0.2	1.45	1.77
1.0	1.41	1.5

These experiments, where rather large values of damping and overstrain are applied, are nevertheless instructive to our understanding of the energetics of brittle versus ductile fracture. For the LJ crystal strained to 5%, we show crack velocity vs γ in Table IV. Crack velocities decrease with increased viscous damping, showing the dynamical effect of dissipation, rather than increased brittleness. In the $\gamma=0.2$ case, the early-time velocity of an emitted dislocation is relatively unaffected by the viscous damping, namely, it is about 90% of the shear-wave speed; similarly, the acoustic pulse emanating from the early bond-breaking events is about 90% of the longitudinal speed.

From these experiments with artificial viscous damping, we conclude that quasistatic cracks in the LJ system are, in fact, brittle. When the strain is raised above the critical value, the crack propagation becomes dynamic—the velocity increases, and the crack tip "heats up." At that point, dislocations can be emitted, and the material becomes ductile. Dynamic crack propagation can therefore be qualitatively different from static predictions.

E. Dependence of critical strain on crack length

We note that the critical strain we have observed appears to be independent of crack length, and to depend instead upon the curvature at the crack tip. In our earliest simulations, we chose to study narrow triangular notches that were about 17 atomic spacings deep and 3 wide, so that the crack surface was not atomically smooth; the critical strain was just a bit above 2%, for samples containing either 30 000 or 300 000 atoms. From this, we can conclude that the critical strain depends only on the initial crack geometry, not the system size, provided that the crack volume is small compared to the total. Then, for a series of long, narrow notches 2 atomic layers wide, we determined the critical strain for crack motion by examining snapshots taken at time intervals of t_0 at a strain rate of $10^{-3}t_0^{-1}$, so that the uncertainty in critical strain was about 0.1%. Critical strain as a function of crack length is presented in Table V. Independently,

TABLE V. Critical strain (%) as a function of crack length (width = $2r_0$).

Crack length (r_0)	Critical strain (%)
68	2.3
46	2.2
23	2.4
10	3.15
6	3.7

Dienes and Paskin[6] found a critical strain of 2.9% for their longest crack of length $10r_0$, compared to our value, 3.15%. However, they stopped at a length which fortuitously agrees with their continuum formulation of the Griffith criterion (predicting that the critical strain depends on the inverse square root of the crack length). From our results, on the other hand, we conclude that for a narrow notch whose length is 20 or more atomic spacings, the critical strain is independent of length.

IV. CONCLUSIONS

Massively parallel molecular-dynamics simulations make it possible to study fracture at the atomistic level in samples that are far more macroscopic in extent than ever before. Nevertheless, the severe time and space limitations of MD—primarily represented by the sound traversal time—require that clever boundary conditions be applied so as to mimic a large system embedded in an "infinite medium." Dynamic crack initiation at finite strain rates is achieved most efficiently by imposing a linear velocity profile transverse to the propagation direction (pointed to by a notch in the sample). A constant strain above the critical value can then be achieved by subtracting off the linear profile and setting the boundary velocities to zero. This gentle ramp-up to the final strain prevents extraneous rarefaction waves caused when a sudden strain is imposed. We have shown that even apparently innocent sound waves reflected from the boundaries can affect crack morphology by inhibiting or healing bifurcations, or by inhibiting the emission of dislocations. We have therefore investigated a number of reservoir methods for absorbing sound waves and dislocations emitted from the crack tip. The best method, which minimizes the mismatch between reservoir and sample, is to gradually ramp up the viscous damping coefficient for reservoir-atom velocities over a distance of about 20 atomic layers.

Over a wide range of strain rates and for temperatures up to at least one-fourth of melting, we observe that the critical strain is nearly a constant for a given material. By introducing an artificial viscous damping mechanism into constant plane-strain fracture simulations, we observed that ductility can be suppressed, so that brittle behavior alone is observed, with a crack velocity that depends on the amount of strain above critical. The amount of dissipation required to inhibit dislocation emission is also roughly proportional to the excess strain. From these experiments, we see that dynamical effects are important in assessing brittleness and ductility. Also, we see that ductile fracture is a thermally activated process. Increasing the strain rate in the case of constant strain-rate simulations, or increasing the supercritical strain in constant plane-strain simulations, results in effectively higher "temperatures" at the crack tip, and leads to generation of higher numbers of mobile dislocations, i.e., ductile behavior.

The interaction potential in the attractive (expansion) region dominates the intrinsic brittleness or ductility of a material at zero temperature. We were able to alter the behavior of an otherwise ductile material by making the attractive potential more short ranged, and thereby the force more strongly attractive. The unexpected complexity of the resulting brittle behavior showed, however, that the distinction between brittleness and ductility is very fuzzy, since the degree to which dislocations are bound to the crack tip depends on the applied strain. Moreover, we note that a crack moving at a nonzero velocity behaves differently from a static one. In dynamic crack propagation, we see that the kinetic temperatures can be locally very high in the vicinity of the crack tip and mobile dislocation cores—approaching the melting temperature.

We restate the distinction between brittle and ductile behavior for dynamical cracks by noting that in brittle materials, dislocations are asymptotically bound to the crack tip, while in ductile materials, the dislocations are asymptotically free. We observe that the early time velocities of the emitted dislocations in ductile materials appear to be approximately the shear-wave speed. The dislocations then slow down far from the crack (at tens of lattice spacings) to a velocity of about two-thirds of the shear speed. We also see that dislocation emission and climb is important in crack forking.

In a forthcoming paper,[20] we will report on our observation that the direction of crack propagation in the 2D triangular lattice can also affect the apparent ductility, that is, the rate of production of mobile dislocations. In the simulations we have discussed so far, we launched cracks in the direction parallel to the close-packed lines—the so-called "natural" cleavage direction. (In the 2D triangular lattice, close-packed "planes" occur in three orientations. These are the three distinct slip directions along which dislocations can move, and they are also the natural cleavage planes.) The 2D lattice is elastically isotropic, so that long-wavelength sound waves travel at the same speed in any direction. However, fracture involves very nonlinear deformation, so that directionality can well affect crack propagation, even in an elastically isotropic medium. We find that the LJ system, which exhibits ductile behavior for dynamic crack propagation along the natural cleavage direction, is much more brittle when a crack is launched perpendicular to the close-packed rows, along which tension is applied. In this case, the formation of dislocations is inhibited, and the crack tends to zigzag rather than blunt. Moreover, the zigzag amplitude is much larger than in the natural direction, where it is typically one atomic layer.

The brittleness observed in this zigzag instability is not too surprising, since in the transverse direction there are two cleavage planes at $\pm 30°$, rather than straight ahead as in the natural cleavage direction. As a consequence, the crack velocity is significantly higher in the transverse direction than in the natural direction. When the strain is ramped up at a rate of 10^{-3}, past the critical strain of 2% in either direction—up to 2.5%—the crack velocity in either case reaches an asymptotic value: the transverse direction velocity is about 2.0, while the velocity in the natural cleavage direction asymptotes at about 1.4 (38% and 27% of the shear-wave speed, respectively). Because of this peculiar directional behavior, one should be cau-

tious about claims that the 2D lattice can be used as a universal example of fracture behavior, particularly as a model for glassy materials that are truly isotropic.[21–23]

In addition to studying polycrystalline materials,[20] we are in the process of applying the fracture simulation approaches we have developed to 3D,[24] where the challenges of adequate boundary treatment and visualization are considerably more severe than in 2D.

ACKNOWLEDGMENTS

Computations were performed on the CM-200 and CM-5 at the Advanced Computing Laboratory at Los Alamos. The authors are grateful to the European Center for Atomic and Molecular Calculations (CECAM) in Paris and its Director, Professor Giovanni Ciccotti, as well as Michel Mareschal, who was co-organizer (with BLH) of a summer (1993) workshop at which many of these fracture issues were studied. Our collaborators, Peter Lomdahl, Niels Jensen, and Dave Beazley, carried out a preliminary 2 000 000-atom constant strain-rate MD simulation to compare with our earliest 32 000-atom calculations. We acknowledge Farid Abraham for collaboration in the early stages of this project, and helpful discussions with John Dienes, John Hirth, Jim Langer, Norm Wagner, Sid Yip, Robb Thomson, Jim Rice, Anders Carlsson, Jim Hammerberg, and Shujia Zhou. Finally, we would especially like to thank Bill Hoover for helpful suggestions in the course of this work and on the manuscript.

APPENDIX A: POTENTIALS

In this appendix, we present potentials we have used—other than Lennard-Jones, Morse, and embedded-atom method potentials, which are presented in the main text.

Johnson potential:[7]

$$\varphi(r)=-ar^3+br^2-cr+d \ , \tag{A1}$$

a	b	c	d	$r_{\min}$	$r_{\max}$
156.296	555.131	629.128	229.831	0	0.91721
45.4964	162.529	188.568	70.5359	0.91721	1.14651
79.3611	279.008	322.114	121.573	1.14651	1.31467
0	0	0	0	1.31467	∞

HAM potential:[1,2]

$$\varphi(r)=\begin{cases}-1+\alpha^2(r-1)^2, & 0<r<r_s \\ -\alpha^2(r_m-r)^2, & r_s<r<r_m,\end{cases} \tag{A2}$$
$$r_m=1+\frac{\sqrt{2}}{\alpha}, \quad r_s=\tfrac{1}{2}(1+r_m) \ .$$

Cubic spline $[r_s\le r\le r_m, \quad \varphi(r_m)=\varphi'(r_m)=0; \ \varphi''(r_s)\neq 0]$:

$$\varphi(r)=\varphi_s+\varphi_s'(r-r_s)+\tfrac{1}{2}\varphi_s''(r-r_s)^2-\tfrac{1}{6}A_3(r-r_s)^3 \ ,$$
$$\varphi_s=\varphi(r_s), \quad \varphi_s'=\varphi'(r_s), \quad \varphi_s''=\varphi''(r_s) \ , \tag{A3}$$
$$r_m=r_s+2\frac{-\varphi_s'+\sqrt{\varphi_s'^2-\frac{3}{2}\varphi_s\varphi_s''}}{\varphi_s''} \ ,$$
$$A_3=\frac{2\varphi_s'}{(r_m-r_s)^2}+\frac{2\varphi_s''}{(r_m-r_s)} \ .$$

Short-range cubic spline $[r_s=r_0=1$ (minimum), $\varphi(r_s)=-1, \ \varphi'(r_s)=0, \ \varphi''(r_s)=2\alpha^2]$:

$$\varphi(r)=-1+\alpha^2(r-1)^2-\tfrac{1}{6}A_3(r-1)^3 \ ,$$
$$r_m=1+\frac{\sqrt{3}}{\alpha}, \quad A_3=\frac{4\alpha^3}{\sqrt{3}} \ . \tag{A4}$$

Intermediate-range cubic spline[13] $[\varphi''(r_s)=0, \ r_s$ is the inflection point]:

$$\varphi(r)=\varphi_s+\varphi_s'(r-r_s)-\tfrac{1}{6}A_3(r-r_s)^3 \ ,$$
$$r_m=r_s-\frac{3\varphi_s}{2\varphi_s'}, \quad A_3=\frac{8\varphi_s'^3}{9\varphi_s^2} \ . \tag{A5}$$

Note on units. It is unfortunate that for our first few calculations, we chose to represent the LJ potential in our MD computer code in the "conventional way," where the unit of distance is the crossing point or zero of the LJ potential $\sigma=r_0/2^{1/6}$. Thus, the careful reader will notice that the strain rates for some of the LJ and EAM calculations are slightly larger, by a factor of $2^{1/6}=1.12$, than in the Morse case, where the unit of distance is naturally r_0. We recommend the abandonment of the "conventional" units for the LJ systems; their *only* utility is to make the 3D close-packed density equal to one, rather than $\sqrt{2}$.

APPENDIX B: RESERVOIRS

In the course of this MD fracture investigation, we examined, albeit in a rather Edisonian fashion, a variety of treatments of atomistic reservoir regions, whose principal purpose is to absorb sound waves and mobile dislocations that have been generated in the process of crack propagation. We chose to restrict ourselves to simple atomistic reservoirs, rather than the more complex methods employed in the past, mainly because the tremendous increase in computer memory afforded by massively parallel computers enables us to use a more brute-force approach. Past methods, even the closely related stress boundary treatment of Yip and co-workers,[5,8,9] have never been implemented on sufficiently large systems to insure that truly boundary-free results have been obtained. This is not to say that coupling of sample atoms to some kind of a continuum treatment, particularly a particlelike method, would not be greatly advantageous in reducing the ratio of reservoir to sample degrees of freedom.

The first continuous-potential, nonequilibrium MD simulation, carried out by Vineyard and co-workers[14] for a radiation damage cascade introduced the use of surface reservoir atoms, whose sole purpose was to damp outgoing shock waves arising from the atom initiating the collision cascade (having been struck by a high-energy neutron). The surface atoms were attached to fixed lattice sites by harmonic springs, and their velocities were damped by viscous dashpots tuned to the critical damping of longitudinal sound waves. In our case, we need to be able to absorb dislocations, too, so that, were we to use the Vineyard group's approach of fixing atoms in the reservoir, we would be preventing dislocation outflow.[5] Thus, in all the methods we considered, we assumed that

the reservoir was open, that is, atoms could enter or leave the reservoir region at will, but once they had crossed over into "no-man's land," anything could be done to their equations of motion. Apart from initial conditions and these boundary conditions, atoms in the central sample region—"the meat" in the sandwich—always obey Newton's equations of motion.

Of the many approaches that we tried for absorbing energy that emanates from the crack-opening process, the unsuccessful ones include the following: velocity rescaling, where the kinetic energy of the reservoir region is controlled at each time step so as to conform to a fixed temperature (in all the thermostatting methods we tried, we subtracted the local expansion velocity from each atom's own velocity, to obtain its peculiar velocity); Nosé-Hoover thermostatting,[15] where, instead of imposing a rigid constraint on the kinetic energy in the reservoir, deterministic feedback ensures that the time-average kinetic energy is equal to the imposed value; introduction of light-mass atoms in the reservoir; and viscous damping, where the peculiar velocity of each atom in the reservoir is damped by a force that is linearly proportional to that velocity, with a single constant damping coefficient for the whole reservoir. All of these methods fail because they look like a hard wall to incoming velocity wave trains, due to the mismatch in dynamics across the reservoir-sample interface. The method that has proved to be successful is *ramped viscous damping,* where the damping coefficient applied to atoms in the reservoir gradually increases linearly from zero (Newton's equations of motion) at the sample interface to a value that critically damps the highest-frequency oscillations at the outer extremity of the reservoir. 1D simulations of a wave train in a harmonic chain showed that, indeed, essentially all frequencies could be absorbed by a reservoir 10–20 atoms thick, with little reflected noise. Though we have not yet extensively employed this technique in 3D fracture simulations, we have used it in a 2D constant-strain simulation, extending the length of run well beyond the sound traversal time. The sound waves are indeed nicely damped and not at all reflected using this reservoir technique.

[1]W. T. Ashurst and W. G. Hoover, Phys. Rev. B **14**, 1465 (1976).

[2]B. Moran, Ph.D. thesis, University of California, Davis/Livermore, 1983.

[3]M. Mullins and M. A. Dokainish, Philos. Mag. A **46**, 771 (1982).

[4]J. E. Sinclair, P. C. Gehlen, R. G. Hoagland, and J. P. Hirth, J. Appl. Phys. **49**, 3890 (1978).

[5]B. deCelis, A. S. Argon, and S. Yip, J. Appl. Phys. **54**, 4864 (1983).

[6]G. J. Dienes and A. Paskin, J. Phys. Chem. Solids **48**, 1015 (1987); K. Sieradzki, G. J. Dienes, A. Paskin, and B. Massoumzadeh, Acta Metall. **36**, 651 (1986); A. Paskin, D. K. Som, and G. J. Dienes, *ibid.* **31**, 1841 (1983).

[7]R. A. Johnson, Phys. Rev. A **134**, 1329 (1964).

[8]S. Yip and D. Wolf, in *Materials Science Forum,* edited by G. E. Murch (Trans Tech Publications, Aemannsdorf, Switzerland, 1989), Vol. 46, p. 77.

[9]K. S. Cheung and S. Yip, Phys. Rev. Lett. **65**, 1804 (1990).

[10]N. J. Wagner, B. L. Holian, and A. F. Voter, Phys. Rev. A **45**, 8457 (1992).

[11]B. L. Holian and D. E. Grady, Phys. Rev. Lett. **60**, 1355 (1988).

[12]A preliminary account of this work appears in B. L. Holian, F. F. Abraham, and R. Ravelo, in *Advanced Computational Methods for Material Modeling,* edited by D. J. Benson and R. J. Asaro (ASME, New York, 1993), AMD-Vol. 180/PVP-Vol. 268, p. 207.

[13]B. L. Holian, A. F. Voter, N. J. Wagner, R. J. Ravelo, S. P. Chen, W. G. Hoover, C. G. Hoover, J. E. Hammerberg, and T. D. Dontje, Phys. Rev. A **43**, 2655 (1991).

[14]J. B. Gibson, A. N. Goland, M. Milgram, and G. H. Vineyard, Phys. Rev. **120**, 1229 (1960). This pioneering work in nonequilibrium molecular dynamics introduced the Størmer (now often called Verlet) integration method, as well as the notion of reservoir regions.

[15]W. G. Hoover, Phys. Rev. A **31**, 1695 (1985).

[16]S. J. Zhou, A. E. Carlsson, and R. Thomson, Phys. Rev. Lett. **72**, 852 (1994).

[17]J. S. Langer and H. Nakanishi, Phys. Rev. E **48**, 439 (1993).

[18]H. J. C. Berendsen, J. P. M. Postma, W. F. van Gunsteren, A. DiNola, and J. R. Haak, J. Chem. Phys. **81**, 3684 (1984).

[19]The Berendsen thermostat was rederived and used in an interesting MD simulation of laser-induced melting of copper: H. Häkkinen and U. Landmann, Phys. Rev. Lett. **71**, 1023 (1993).

[20]R. Ravelo, S. J. Zhou, and B. L. Holian (unpublished).

[21]F. F. Abraham, D. Brodbeck, R. A. Rafey, and W. E. Rudge, Phys. Rev. Lett. **73**, 272 (1994).

[22]M. Marder and X. Liu, Phys. Rev. Lett. **71**, 2417 (1993).

[23]A. Yuse and M. Sano, Nature **362**, 329 (1993); J. Fineberg, S. P. Gross, M. Marder, and H. L. Swinney, Phys. Rev. Lett. **67**, 457 (1991).

[24]P. S. Lomdahl, D. M. Beazley, N. G. Jensen, R. Ravelo, S. J. Zhou, and B. L. Holian (unpublished).

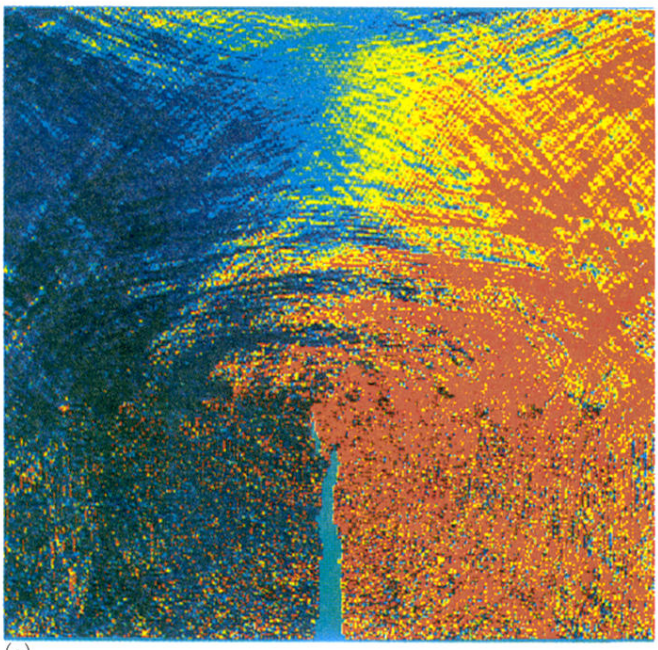

(a)

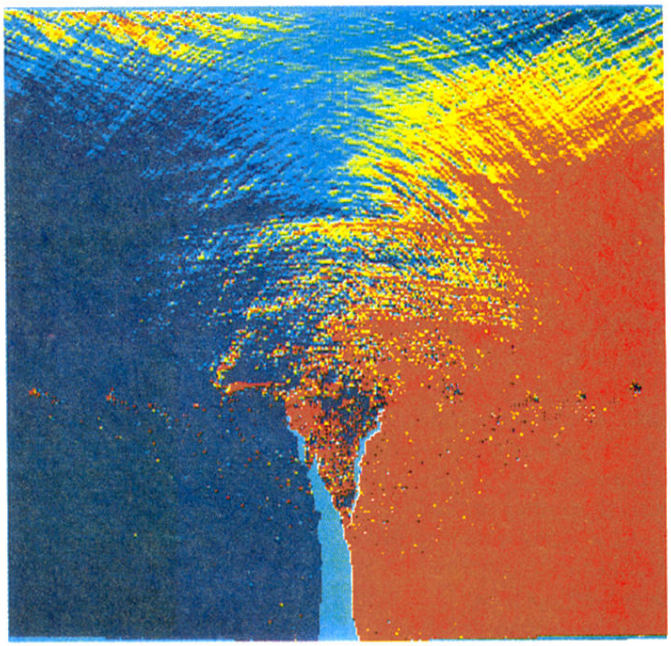

(b)

(c)

FIG. 2. Comparison of system-size (periodic boundary condition effects) on crack propagation at constant strain rate (10^{-4}) in the 2D LJ crystal at time $t = 312t_0$ for two system sizes: (a) 300 000 atoms, aspect ratio (horizontal/vertical) = 1, entire sample shown; (b) 600 000 atoms, aspect ratio = 2, middle half of sample shown—same area as in (a). Constant strain simulation (3%) for 250 000 atoms at $t = 75t_0$ after crack initiation is shown in (c); ramped viscous damping is applied at left and right boundary regions (each 20 atomic layers thick).

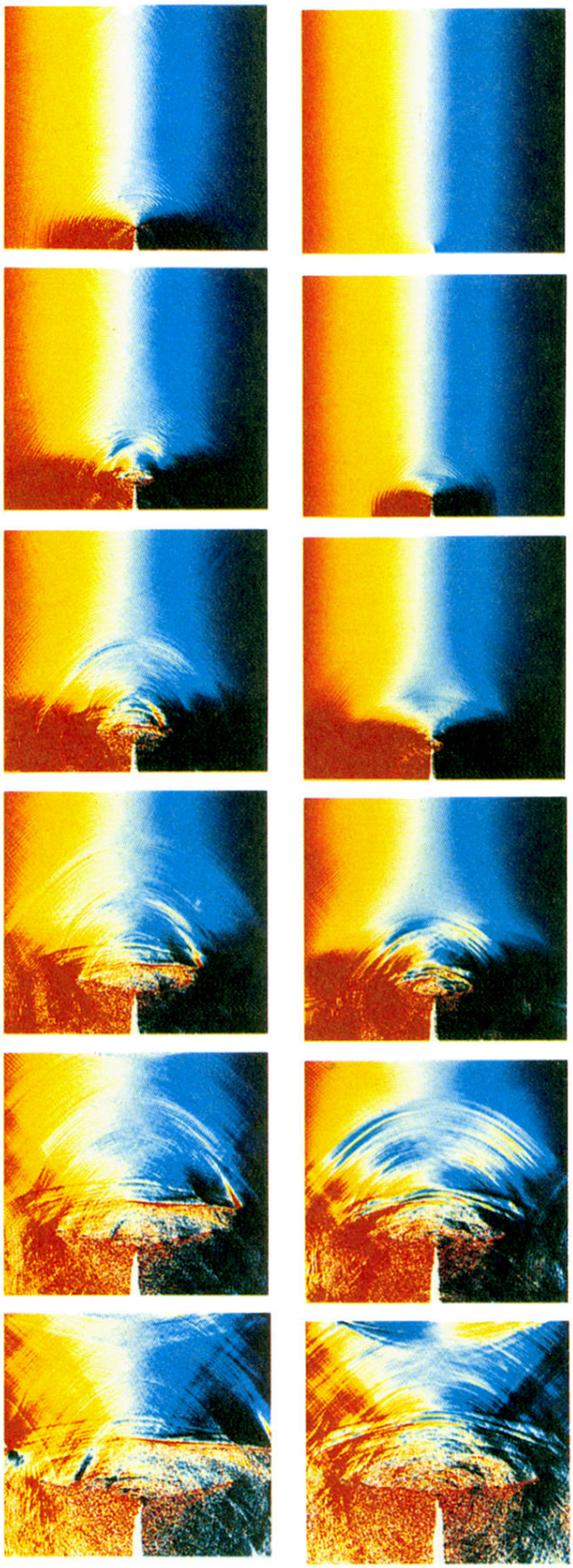

FIG. 3. MD simulations of 2D fracture at constant strain rate (10^{-4}) for Morse pair potential (time sequence $t = 275-400t_0$ on left-hand side) and many-body EAM potential (on right-hand side, $t = 245-356t_0$).

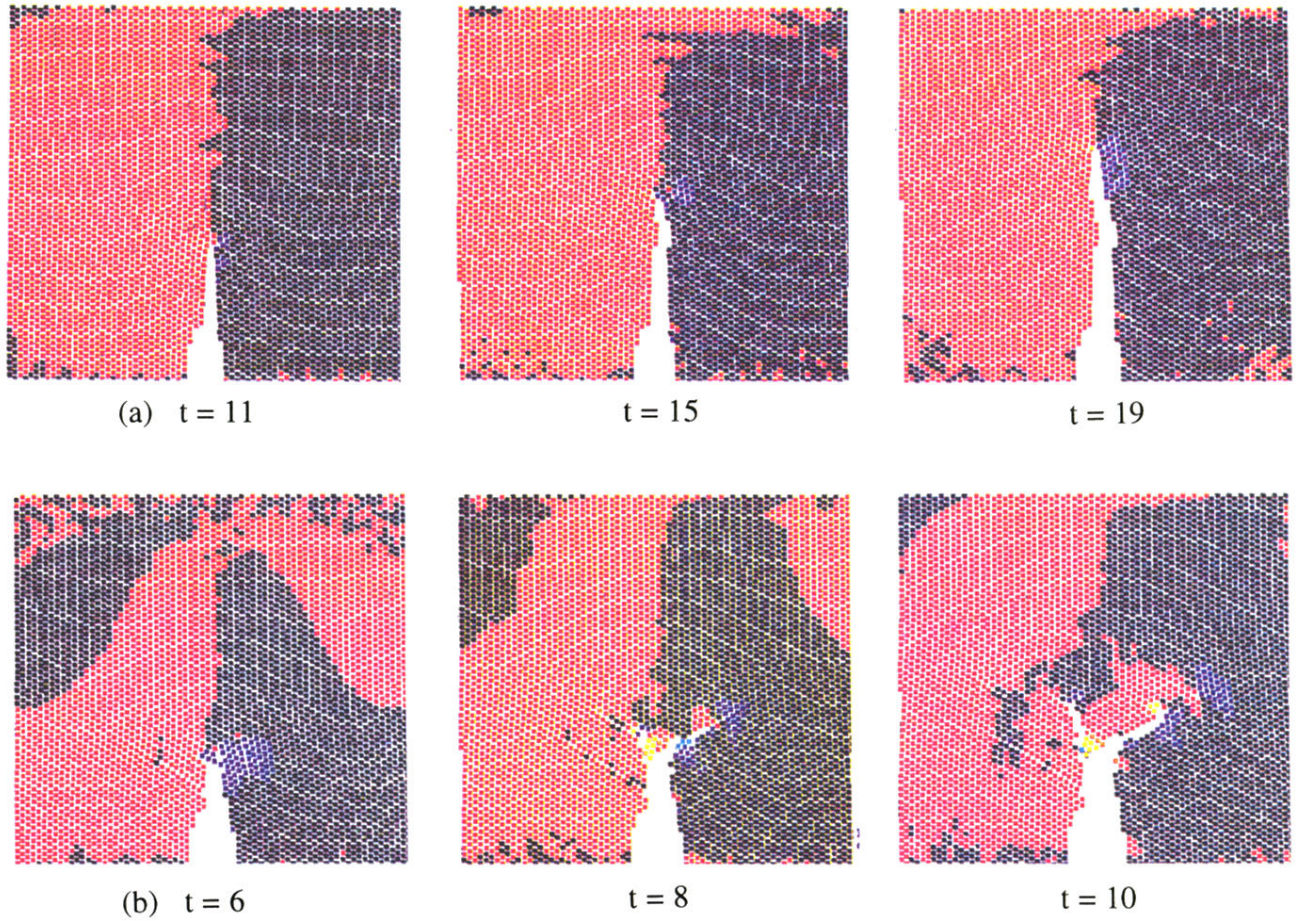

FIG. 7. Brittle fracture (*without* viscous dissipation) in a 2D crystal whose atoms interact via the short-range LJ spline potential. (a) Grain map emphasizing dislocation cores (atoms colored by 60°-periodic rainbow according to orientation of hexagon of nearest neighbors: red at vertical, green at 30° to right, blue at 60°) shown for initial strain of 3% in the horizontal direction at $t = 11$, 15, $19t_0$; (b) initial strain of 6%, for $t = 6$, 8, and $10t_0$.

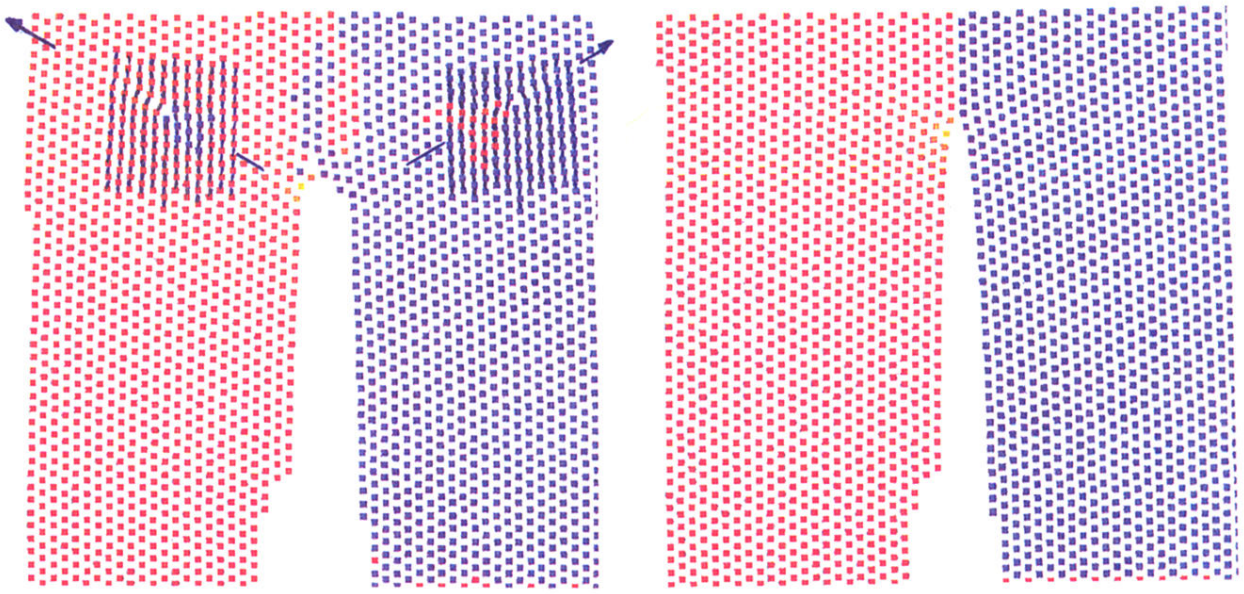

FIG. 8. Effect of viscous dissipation on ductility (grain map as in Fig. 7) in the 2D LJ crystal, prestrained in the horizontal direction to 5%; (a) viscous damping coefficient $\gamma=0.2$ at $t=22t_0$ (note pair of dislocations along $\pm 60°$ slip lines); (b) $\gamma=1$ at $t=30t_0$ (brittle crack).